DOI of final article - https://doi.org/10.1016/j.jeurceramsoc.2021.03.045

Experimental Investigation and Mathematical Modelling of Water Vapour Corrosion of Ti_3SiC_2 and Ti_2AlC Ceramics and their Mechanical Behaviour

Karthikeyan Ramachandran[1], Zuccarini Carmine[1], Katsumi Yoshida[2], Toru Tsunoura[2] and Doni Daniel Jayaseelan[1]*

[1]Department of Aerospace and Aircraft Engineering, Roehampton Vale Campus, Kingston University London, United Kingdom, SW15 3DW.

[2]Laboratory of Advanced Nuclear Energy, Institute of Innovative Reaseach, Tokyo Institute of Technology, Tokyo, Japan

Abstract

Commercially available Ti_3SiC_2 and Ti_2AlC ceramics were used in this study to investigate their wet corrosion and mechanical behaviour as they were under investigation for years for their applications in the field of nuclear as cladding materials and aerospace. The test coupons of dimension 3 x 4 x 40 mm^3 and 3 x 4 x 20 mm^3 were machined out from commercially available samples for the 3-pt bend test and wet corrosion test, respectively. The water vapour corrosion studies of these samples were carried out at 800°C, 1000°C, 1200°C for 10, 20 and 100h in gas flow condition containing 50% steam + 50% air. Phase analysis of the as-received Ti_3SiC_2 and Ti_2AlC ceramics revealed the presence of other impurity phases such as TiC and $TiSi_2$. The XRD patterns of the oxidised samples show the formation of rutile as the major phase in both materials. The oxidation layer formed on Ti_3SiC_2 sample was measured to be 280μm after exposing the sample in steam for 100h at 1200°C. The water vapour corrosion studies reveal that Ti_2AlC has high oxidation resistance compared with the Ti_3SiC_2 due to the formation of protective layers of TiO_2 and Al_2O_3 which resulted in reduced weight gain and oxidation layer thickness. Three-point bend tests were conducted at room temperature for the samples after the water vapour corrosion test at 1000°C/100h. The TAC samples showed no degradation in the bending strength (244MPa) whereas the TSC samples showed reduced strength of 320MPa . The tensile strength of the samples was measured at room temperature and hydrothermal condition (250°C and 250 bars pressure) and it was observed that Ti_3SiC_2 had high tensile strength (190 MPa) in hydrothermal conditions. The tensile strength results were validated using Finite element analysis (FEA) using ANSYS and the FEA results showed a negligible variance of 7% compared with experimental method. Mathematical modelling based on one dimensional solution of diffusion equation combined with Deal-Grove model was

employed to study and compare the oxidation thickness for the linear and parabolic models for the ceramics. The model was effective in validating the oxidation thickness of Ti_3SiC_2 showing that the experimental thickness was closer to that of mathematical model.

Keywords: Ti_3SiC_2; Ti_2AlC; water vapour corrosion; scanning electron microscopy; X-ray diffraction; EPMA; FEA; mathematical modelling.

Corresponding Author: ***Dr Doni Jayaseelan Daniel***

Email: d.daniel@kingston.ac.uk

Introduction

The MAX phase materials have been existed for a long time and there have been numerous studies on the fabrication and synthesis of these materials. Being one of its kind, the MAX phase compounds have provided a great deal of application due to high fracture toughness and oxidation resistance [1]. Some research has been carried out on the MAX phase compounds for gas turbine and nuclear cladding applications due to their combined properties of ceramics and metals [2, 3]. The application of MAX phase materials was discussed for applications include engine cylinders, electrical contacts, heat exchangers, etc [4]. M Li and X Zhou *et al.* have proposed Ti_3SiC_2 as an interphase material in the field of nuclear reactors for SiC/SiC composites [5, 6]. The MAX phase compounds have been also proposed for high temperature applications like protective covers, low friction surfaces and electrical systems by some researchers [7]. The high damage tolerance, chemical resistance and temperature capabilities of the MAX phase has made it a suitable material in field of nuclear cladding and aerospace applications [6, 8]. In nuclear reactors, the oxidation of zircaloy due to loss of cooling in steam condition could lead to release of hydrogen which can cause explosion after the accidents. MAX phase material provides oxidation resistance similar to that of ceramics along with high thermal conductivity as that of metals which makes them a suitable replacement for the job [9, 10].

In this work, the water vapour corrosion studies of Ti_3SiC_2 (hereafter will be referred as TSC throughout the text) and Ti_2AlC (hereafter will be referred as TAC throughout the text) were carried out for different lengths of time using a tube furnace with temperature being a dependent. The mechanical behaviour of the composites was also evaluated. The finite element analysis (FEA) was also utilised to validate the tensile properties obtained from experimental method. A mathematical model was also developed with help of diffusion and Deal-Grove growth equations to validate the oxidation thickness of the samples.

Experimental Methods

Water Vapour Corrosion Studies

The commercial blocks of TAC and TSC were cut into different sizes of 3 x 4 x 20 mm^3 and 3 x 4 x 40 mm^3. The cut coupons were polished down to 1 μm finish before the test using diamond slurry. The water vapour corrosion tests were carried out for both TSC and TAC samples in a tube furnace for different lengths of time (10h, 20h and 100h) at different temperatures (800, 1000 and 1200°C). For the water vapour corrosion study, the samples were placed on an

alumina boat (Figure 1a) and corrosion study was conducted in steam environment (Figure 1b). The alumina boat was utilised to reduce the direct contact between the alumina surface and the samples. But to have a minimum contact between the boat and samples, the samples were placed in a wedged angle as a small groove was made on the walls of the alumina boat. The Pt/Pt-Rh thermocouple was used to measure the temperature of the samples which were placed exactly at the centre of the furnace. The corrosion experiment was carried out at 1 atm. pressure with a gas (50% air + 50% water) flow rate of 400mL/min. Figure 1b shows the temperature profile and gas flow of the corrosion experiments. Initially, the furnace was purged with Ar gas to remove any contaminant. The furnace was heated up to maximum temperature at the rate of 5°C/min in Ar atmosphere up to the maximum temperature. This was to avoid any oxidation before the experimentation temperature. Once the test temperature was reached, the steam (50% air+50% water) was introduced into the furnace and similarly during cooling process, the gas supply was switched back to Ar to avoid further oxidation.

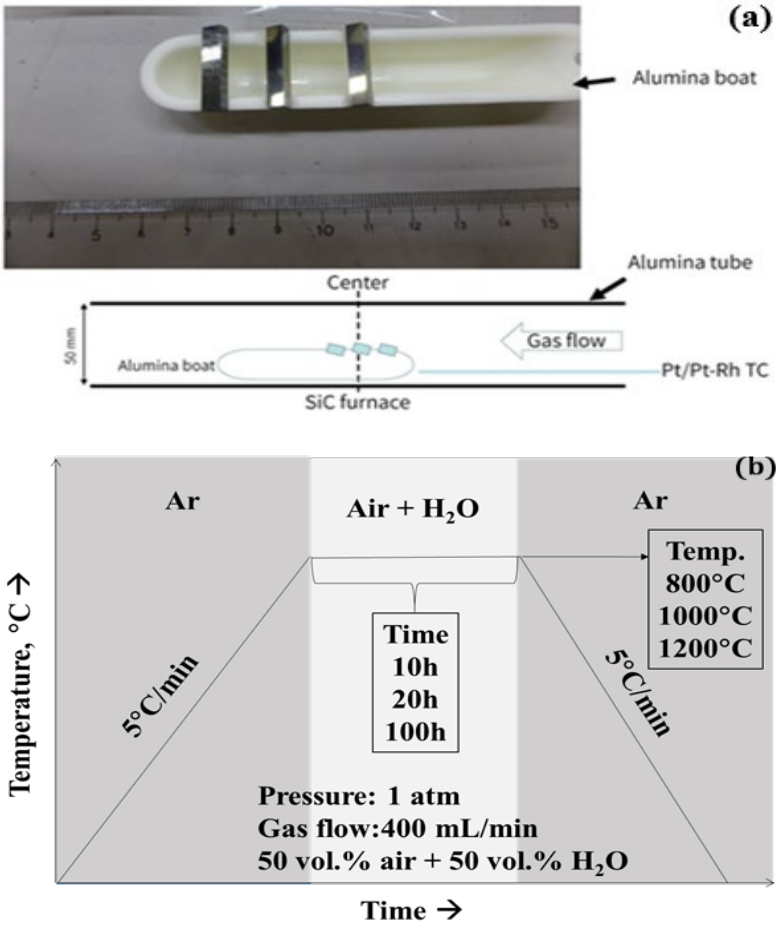

Figure 1. (a) Samples on the alumina boat & schematic of the experimental setup and (b) Temperature profile for water vapour corrosion experiments

Characterisation

The Scanning Electron Microscope (S-4800 Hitachi) was used to analyse the surface microstructures and the cross-section of the samples. The X-ray diffractometer (RINT-Ultimalll, Rigaku) fitter with CuK_{α} was used to analyse the phases present on the surface before and after corrosion studies. The electron probe micro-analyser (EPMA) was utilised to study the composition of the materials using JXA-8800RL, JEOL.

Mechanical Testing

Tensile test according to ASTM standards (ASTM D3039) was performed at room temperature and at hydrothermal condition (250 bar & 288°C) for both TSC and TAC samples. Under hydrothermal condition, the tensile samples were heated for 100 h. The loading rate for the tensile test was kept at 0.2kN/min. The tensile strength, fracture strength and mass changes were determined after the test. The tensile strength and fracture strength of the materials were calculated using the formula given below.

Tensile Strength

$$\sigma = \frac{F}{A_o} \tag{1}$$

Fracture Strength

$$\sigma_f = \frac{F_f}{A_f} \tag{2}$$

where F is the tensile force, F_f is the fractural force acting on the material and A_o and A_f are the original area and fracture area of the samples, respectively. The bend tests were carried out for the samples having dimension 3×4×40 mm^3 with crosshead speed of 0.5 mm/min to determine the retained strength after the oxidation. The samples were placed on the jig in such a way that the oxidised surface was at the bottom under tension during the test.

Finite Element Analysis

Finite element analysis was carried out using static structural in ANSYS 19.2 with an equal mesh size for both conditions of tensile testing to compare the results with experimentally obtained values. The boundary conditions and environmental conditions in the finite element software were set to closely match up the experimental testing conditions.

Results & Discussion

Ti_2AlC

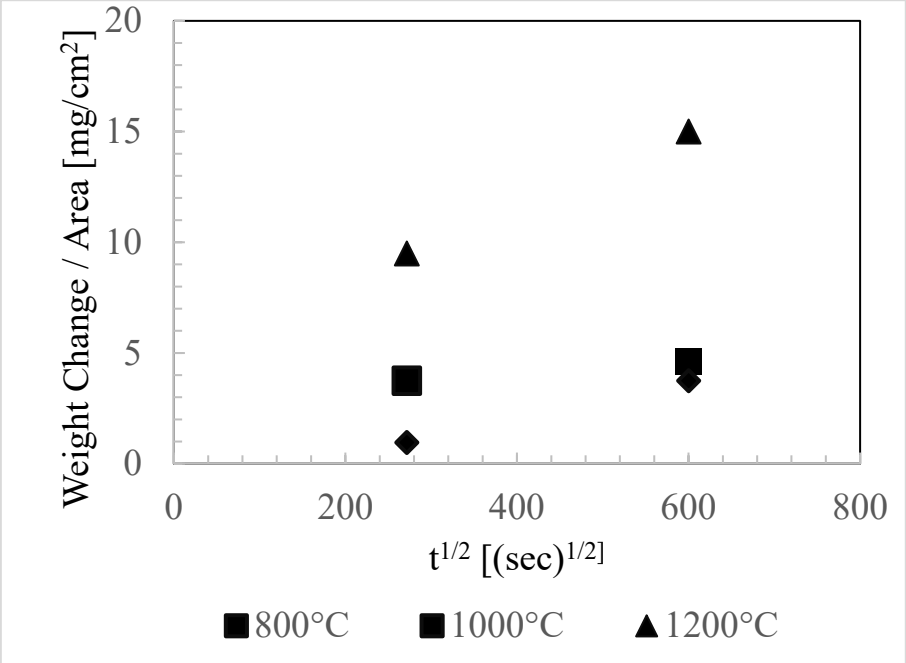

Figure 2. Corrosion test of TAC: Weight change per unit area with respect to time

Figure 2 shows the weight change per unit area for the water vapour corrosion tested TAC samples as a function of the square root of the exposure time at 800, 1000 and 1200°C in presence of 50% air + 50% water. It can be observed that there is negligible or no weight change per unit area (0.96 mg/cm^2) for TAC sample for 20h hold time at 800°C and there is a slight increase in the weight gain per unit area for 100h hold time (3.753 mg/cm^2). At 1000°C, there is an increased weight change (3.753 mg/cm^2) initially for 20 hold time and then it remains constant or increased little (4.6 mg/cm^2) for 100h. This might be due to the formation of the protective layer at 1000°C. The plot in Figure 2 reveals that the weight gain per unit surface area for the samples tested at 800°C and 1000°C was negligible even after 100 h. The negligible weight gain proves that the samples have good oxidation resistance. However, for 1200°C tested samples, the weight gain per unit surface area is slightly high (9.5 mg/cm^2) and it increased to 15 mg/cm^2 for 100h, when compared with the samples tested at 800°C and 1000°C.

To further understand the weight gain after oxidation, phase and microstructure analyses of the TAC samples were carried out. Figure 3 shows the XRD patterns of top and side surfaces of the as received and polished TAC samples prior to oxidation. The XRD pattern of TAC

specimen reveals that the peaks intensity prior polishing is small with noises, which may be due to uneven surface finish of the commercial samples. However, after mirror polishing the samples shows well-defined peaks of TAC. As marked in the Figure 3, peaks correspond predominantly to TAC phase and there has been a presence of $TiAl_3$ at 2 theta = 25, 38, 42 and 75 degree, which shows that the commercially bought TAC sample is not pure.

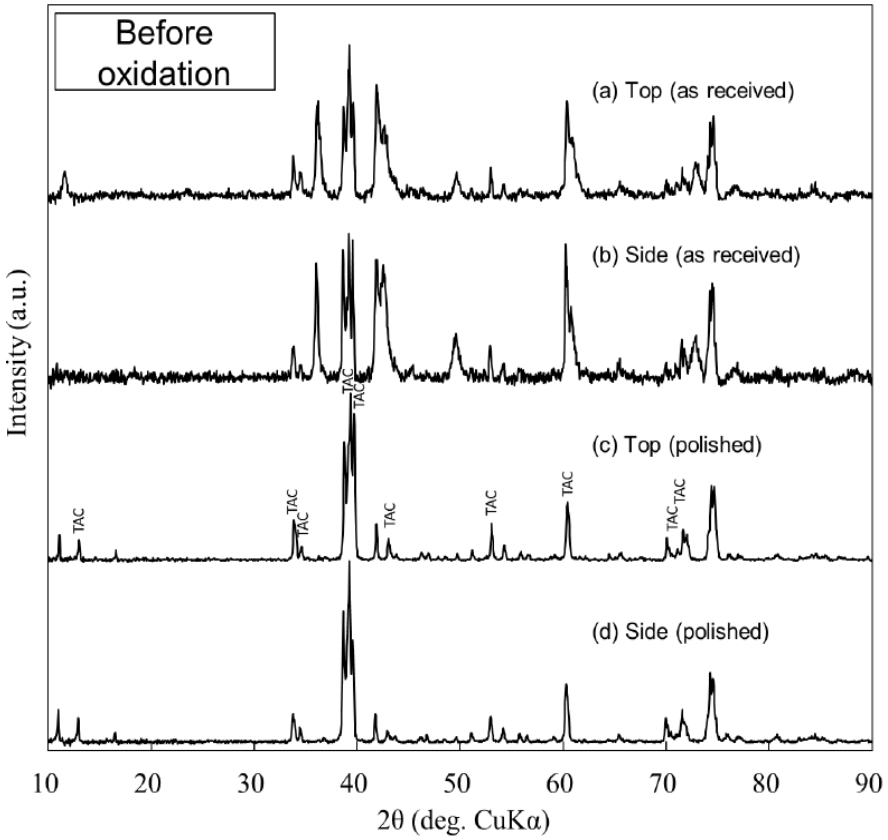

Figure 3. XRD patterns of top and side surfaces of as received and polished TAC sample

Figure 4 shows the XRD patterns of the TAC sample after corrosion for 20 h for 3 different temperatures. It is observed from Figure 4 that there was no oxidation for 0h at 800, 1000 and 1200℃. However, the TAC samples underwent oxidation for 20h at 800℃, 1000℃ and 1200℃. At 800℃, TiO_2(rutile) and Al phases start to appear on the surface of the sample. At 1000℃ and above, alumina phase starts to appear along with rutile and Al phases. In all three temperatures, the presence of TAC phase is observed which clearly indicates that the TAC phase is not completely oxidised in the presence of water vapour in this temperature regime. The formation of TiO_2 (rutile) has been observed from the beginning of oxidation but as the temperature is increased, the presence of rutile phase is not visibly seen but leading to formation

of α-Al_2O_3. The presence of Al in all samples can be reasoned out to reduction of Al_2O_3 in the presence of low oxygen partial pressure [11].

$$2TiAlC + H_2O(g) + 5O_2 \rightarrow 2TiO_2(Rutile) + Al_2O_3 + 2CO_2(g) + H_2(g) \quad (3)$$

$$2Al_2O_3 + 3C(g) \rightarrow 4Al + 3CO_2(g) \quad (4)$$

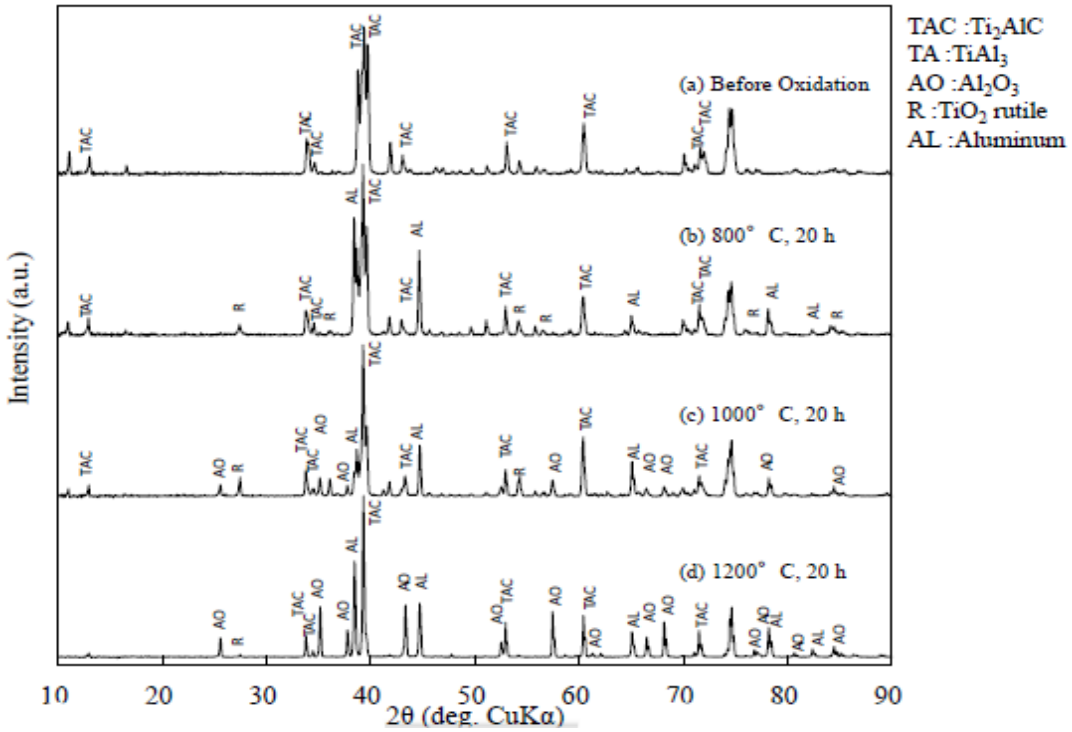

Figure 4. XRD patterns of TAC samples after water vapour corrosion study at 20h at 800°C, 1000 and 1200°C; where, AO: Alumina; R: Rutile structured Titanium dioxide, Al: Aluminium

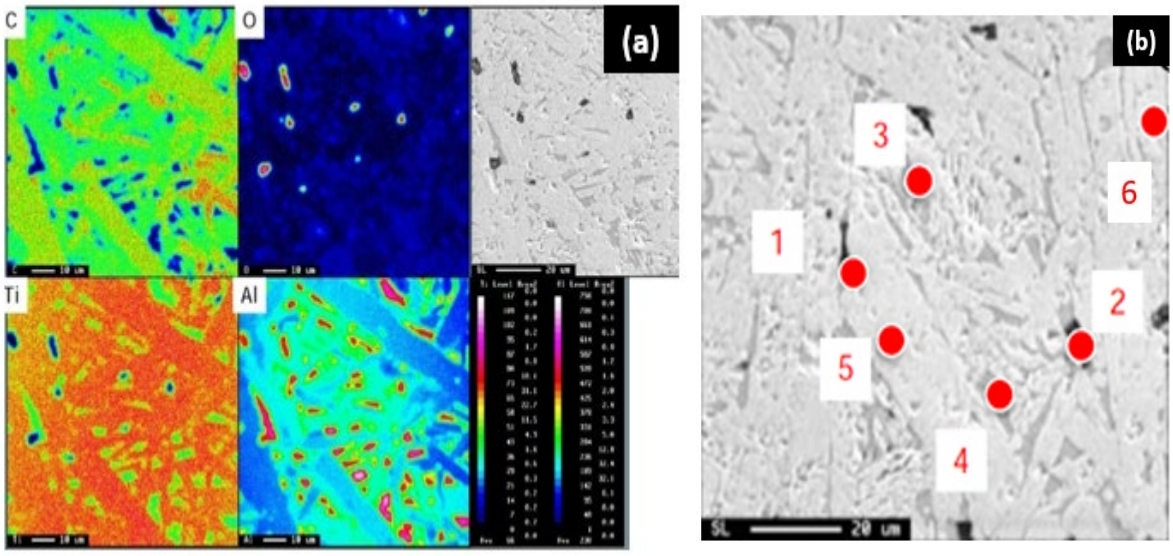

Figure 5. (a) EPMA of TAC sample prior to oxidation (b) point based EPMA of TAC

The elemental analysis of the TAC samples was studied using EPMA technique before and after oxidation. The electron image in Figure 5(a) shows the elongated morphology of TAC grains on the surface. It is evident from Figure 5 that the TAC comprises of mainly Ti, Al, C and small traces of oxygen which may be present on the surface/atmosphere. EPMA was carried out on the surface of the sample at six different points. The elemental composition of TAC prior to oxidation is tabulated in Table 1. The results of EPMA (Figure 5(b)) shows the presence of Al_2O_3 + TiC, $TiAl_3$ and TAC which were not picked by the XRD. The presence of intermediate phases like Al_2O_3 and $TiAl_3$ confirms again that the sample is not pure and has some impurities present in it. The Figure 6 shows EPMA of cross-sectional image of TAC samples oxidised for 20 h at 800°C. After 20 h of oxidation, there is a formation of an intermediate Ti depleted aluminium oxide layer.

Table 1. Composition of Chemical present Before Oxidation in TAC

Point	C [at %]	O [at %]	Al [at %]	Ti [at %]	Phase
1	6.31	57.32	27.42	8.95	Al_2O_3 + TiC
2	7.64	55.60	32.58	4.18	Al_2O_3+ TiC
3	5.42	7.96	57.32	29.33	$TiAl_3$
4	4.10	9.94	56.24	29.71	$TiAl_3$
5	23.77	9.67	17.16	49.40	TAC
6	20.84	6.95	21.62	50.58	TAC

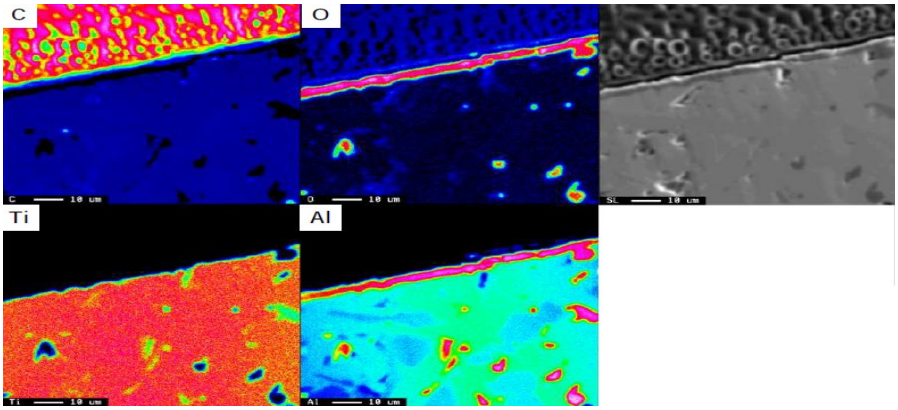

Figure 6. Cross-sectional EPMA of TAC sample after water vapour corrosion study at 800°C for 20 h

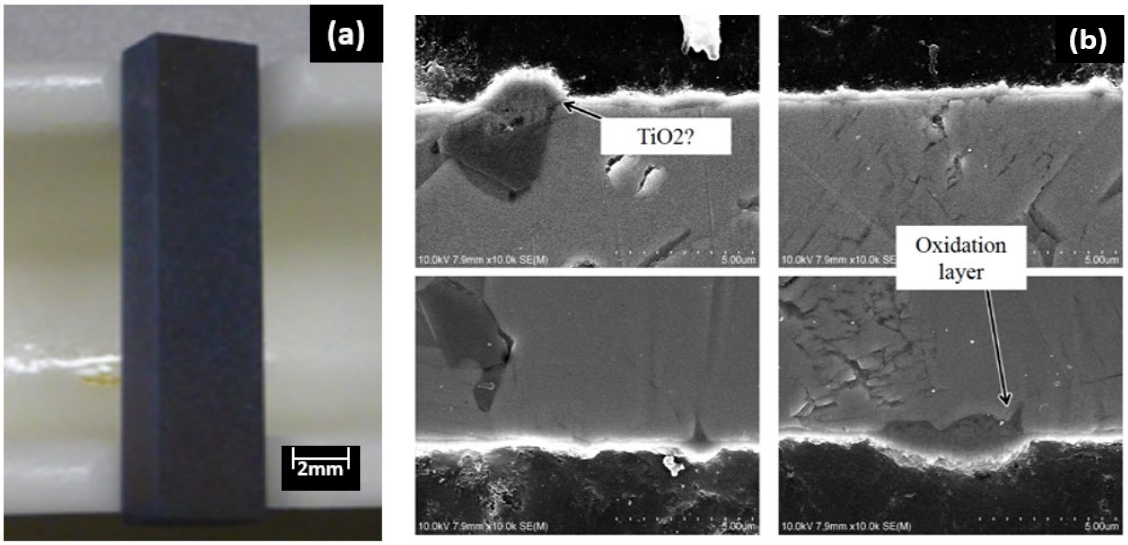

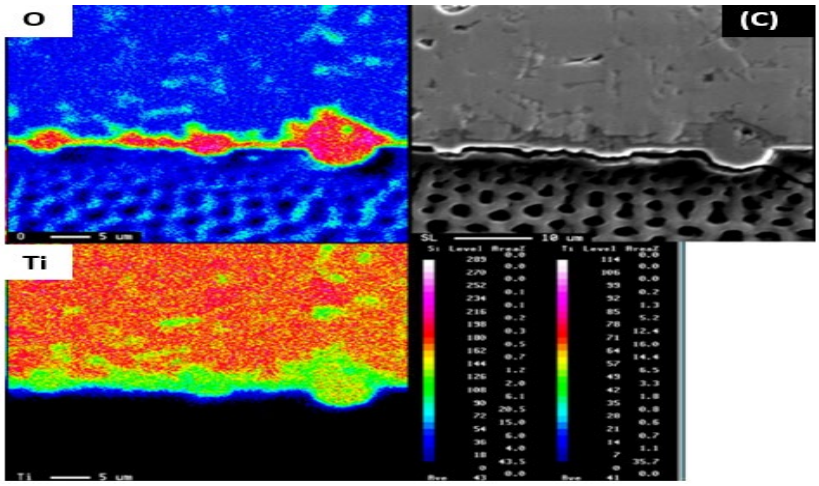

Figure 7. (a) Optical image of TAC sample after water vapour corrosion at 800°C at 100 h (b) SEM image of oxidation layer formed in the TAC sample at 1200°C at 20 h (c) Cross sectional EPMA confirming presence of TiO_2 in TAC sample at 1200°C at 20 h

Figure 7(a) shows the optical image of TAC samples and it is evident from observation that material after oxidation did not undergo any deformation in the structure and its shape have been maintained throughout the tests. The SEM image (Figure 7(b)) shows formation of oxide layer throughout the surface . Also, there have been formation of localised bulk particles of TiO_2 (Figure 7(b) & 7(c)) at the surfaces and formation of continuous protective layers of Al_2O_3 scales which have been due to the selective oxidation of Al present in the TAC which were observed even in our previous studies [12, 13].

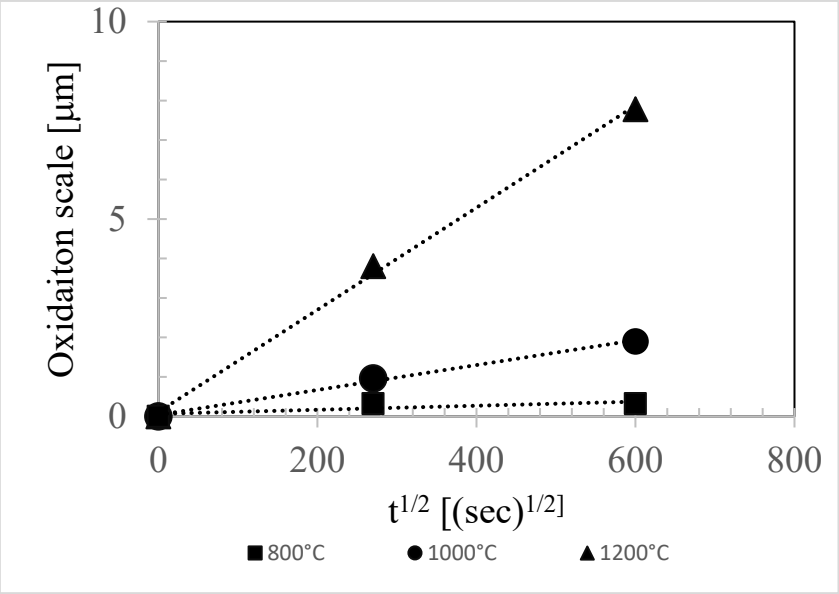

Figure 8. Oxidation kinetics of TAC material under different temperature

From the Oxidation kinetics of TAC samples, it is evident that the material follows parabolic law of oxidation behaviour. According to Wagner's theory, an oxidation behaviour could be said to be parabolic if the scale of diffusion, mass gain and expose time could be described as

$$\left(\frac{\Delta W}{A}\right)^2 = K_p t \qquad (5)$$

Where K_p is the parabolic constant, A is surface area of sample, ΔW is mass gain and t is expose time. Fig 8 presents the oxidation kinetics of the TAC samples under different interval of time with dependency towards temperature. It is obvious from the Fig 8 that the specimen follows the parabolic rate law as the plot shows a straight line. Also, it was believed that the oxidation of TAC followed inward diffusion of the oxygen forming up the TiO_2 and α-Alumina in process. But in dry environment, the TAC samples did not follow the parabolic law rather it was assumed to followed near-cubic rate law in the temperature range of 1100-1300℃ [11]. This was similar to works oxidation kinetics of Ti_3AlC_2 in dry environment [14]. Wang *et al.*

studied TAC ceramics under dry condition at different temperatures and intervals and concluded that the material does not follow parabolic law till a temperature of 600℃. But after 600℃, the oxidation of TAC material follows parabolic law in dry conditions [15]. But in this study, from the oxidation kinetics of TAC in water vapour environment as shown in Figure 8, it was observed that the material follows the parabolic law of oxidation with measured activation energy of 199 KJ/mol and frequency factor of $1.88\times10^{-9}m^2s^{-1}$. The oxidation process was proceeded by inward diffusion of oxygen. It is also believed that the reaction of TAC with H_2O is less intense when compared with the oxidation of TAC in presence of air. So, the weight gain until the temperature of 1000℃ was less compared with mass gain at 1200℃ in presence of water vapour environment. But Z.J. Lin *et al*. reported the same reason for less weight gain in presence of 10% H_2O and 90% air, but he stated that the oxidation followed cubic law at a temperature above 700℃ with minimal weight gain. They also reported that after 1200℃ the water vapour has accelerated the oxidation rate when compared with dry environment which was visible in the oxidation kinetics of TAC material in Figure 8 [16]. While understanding the similarities between the water vapour environment and dry environment, it was obvious that in both case the formation of continuous layers of α- Al_2O_3 was observed in the same temperature range with slower kinetics than the air environment [14]. But in case of water vapour environment, there was some formation of rutile structured TiO_2 lumps on the surfaces (Fig 7(b)) which was due to non-dominate oxidation of TAC at 800℃. By observing the XRD patterns prior and after oxidation, the TAC phases are present even at the temperature range of 800-1200℃. It was obvious from the XRD patterns that the oxide layers formed mainly consisted of rutile structured TiO_2 and α-Al_2O_3 and also the peak intensities of the TAC samples did not reduce after 1200℃ which means that the oxide layer formed on the surface was thin and would have possibly increased with time and temperature. It can also be said that the formation of TiO_2 and α-Al_2O_3 on the surface of TAC specimen acted as a protective layer inhibiting further corrosion. The EPMA shown in Fig. 6 describes the lumps of TiO_2 and layer of Al_2O_3 formed after the oxidation at 800℃. The observation of microstructure of the TAC samples led to a conclusion that the formation of TiO_2 is halted after a certain period whereas the formation of α-Al_2O_3 continuous further with being in the corrosive environment. This have been due to the negative Gibbs energy needed for the formation of Al_2O_3 from the surfaces in the thermodynamic point of view. While observing the chemical point of view, it can be said that energy needed to break the covalent bond of Ti-C would have been more compared to the energy needed to break the metallic bond between Al and Ti. So, formation of Al_2O_3 is being

observed in all the water vapour corrosion environment along with the non-reduced peaks of TAC which shows the oxidation resistance of TAC samples in water vapour environment [17].

Ti_3SiC_2

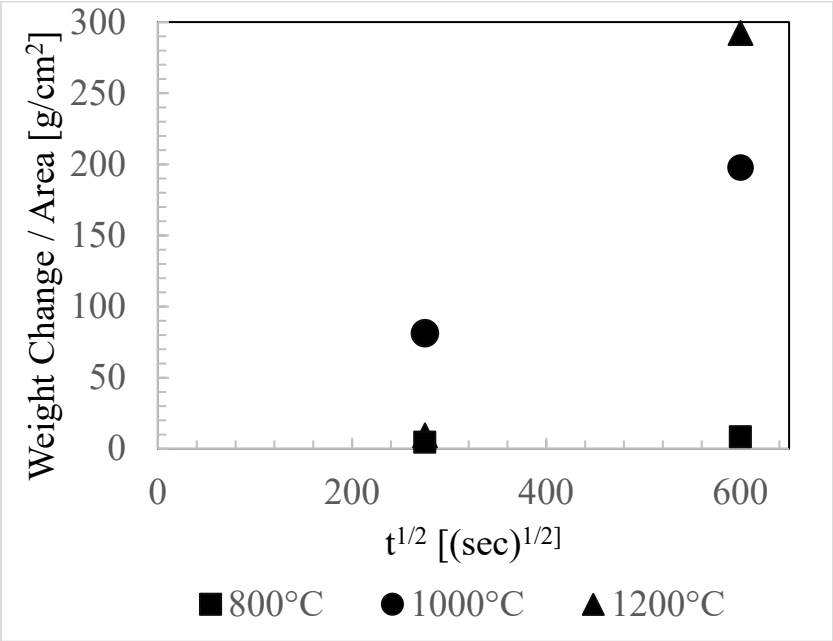

Figure 9. Weight change of TSC samples after oxidation

The Figure 9 shows the plot between the weight change per unit surface area and the square root of time of the TSC. There was no gain observed for the TSC sample tested at 800°C even after 20h, and even after 100h, there was a feeble change in the weight. But the water vapour corrosion of the TSC specimen led to significant weight gain after oxidation at 1000°C. Parabolic oxidation behaviour was followed by the TSC samples during the isothermal oxidation process. At 1000 and 1200℃, the weight gain record (Figure 9) shows that the samples oxidised excessively. The microstructure and XRD of the samples were verified to further investigate the oxidation and weight gain on the samples.

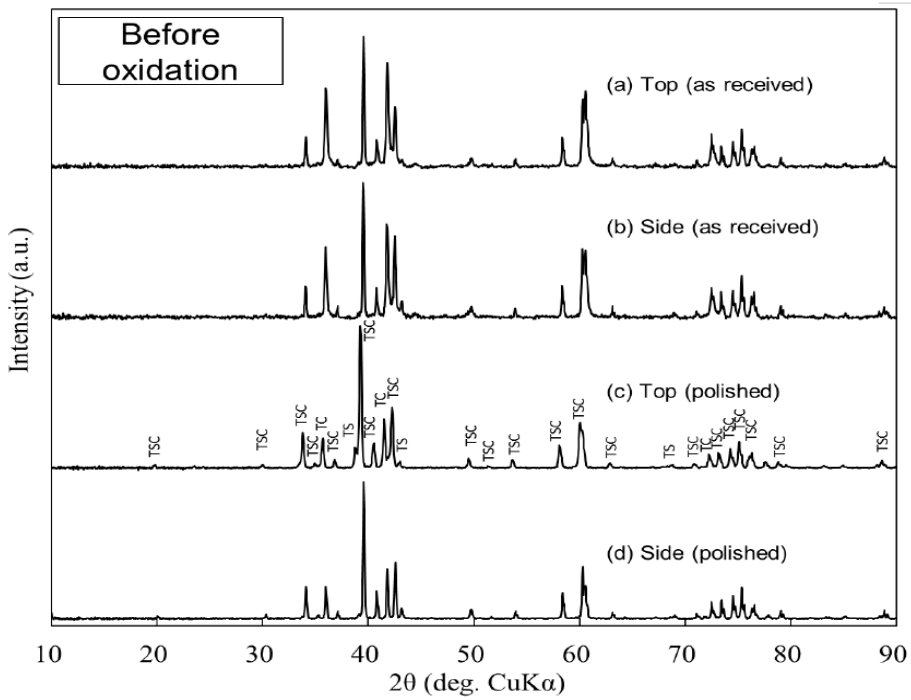

Figure 10. X-Ray Diffraction patterns of top and side surfaces of as received and polished (Ti_3SiC_2) TSC samples.

Figure 10 shows the XRD patterns of the top and side surfaces of the as received and polished samples of TSC prior to oxidation. Even before polishing the XRD patterns of as received sample show peaks with less noise and high intensities. The peaks present for the polished samples were predominantly TSC phase. The XRD also reveals the presence of small trace of TiC (represented as TC in XRD Figures) and $TiSi_2$(represented as TS in XRD Figures) proving that the commercial samples were not 100% pure. Figures 11(a) & (b) show the XRD phases of oxidised at 800℃ and 1200℃ at different lengths of time. The XRD phases in Fig 11(a) reveals that the material did not oxidise at 0 h for any interval of time, but it has started to oxidise when tested for 20h at 800℃ by forming Al, TiO_2 and TS phases. The lack of SiO_2 phase in all the three temperatures range shows the amorphous nature of the material which have been consistent with other research [18, 19]. The XRD patterns at 1200°C revealed that the material shown presence of Al and Rutile TiO_2 after 20 h of oxidation. The presence of Al in TSC sample was believed to be the reaction of Al_2O_3 boat on which wedged samples were kept for the water vapour corrosion. With steam being released at a 50% water and 50% air, there could have been a possibility of hydrogen from the water reacted with Al_2O_3 forming Al [20] as shown in the equation 6. But the Al phase was not observed though the microscopy or chemical analysis which proves that the presence of Al would be due to reduction of Al_2O_3 though hydrogen which settled on the wedge area and were characterised by XRD.

$$Al_2O_3(s) + 6H(g) \leftrightarrow 2Al(g) + 3H_2O(g) \quad (6)$$

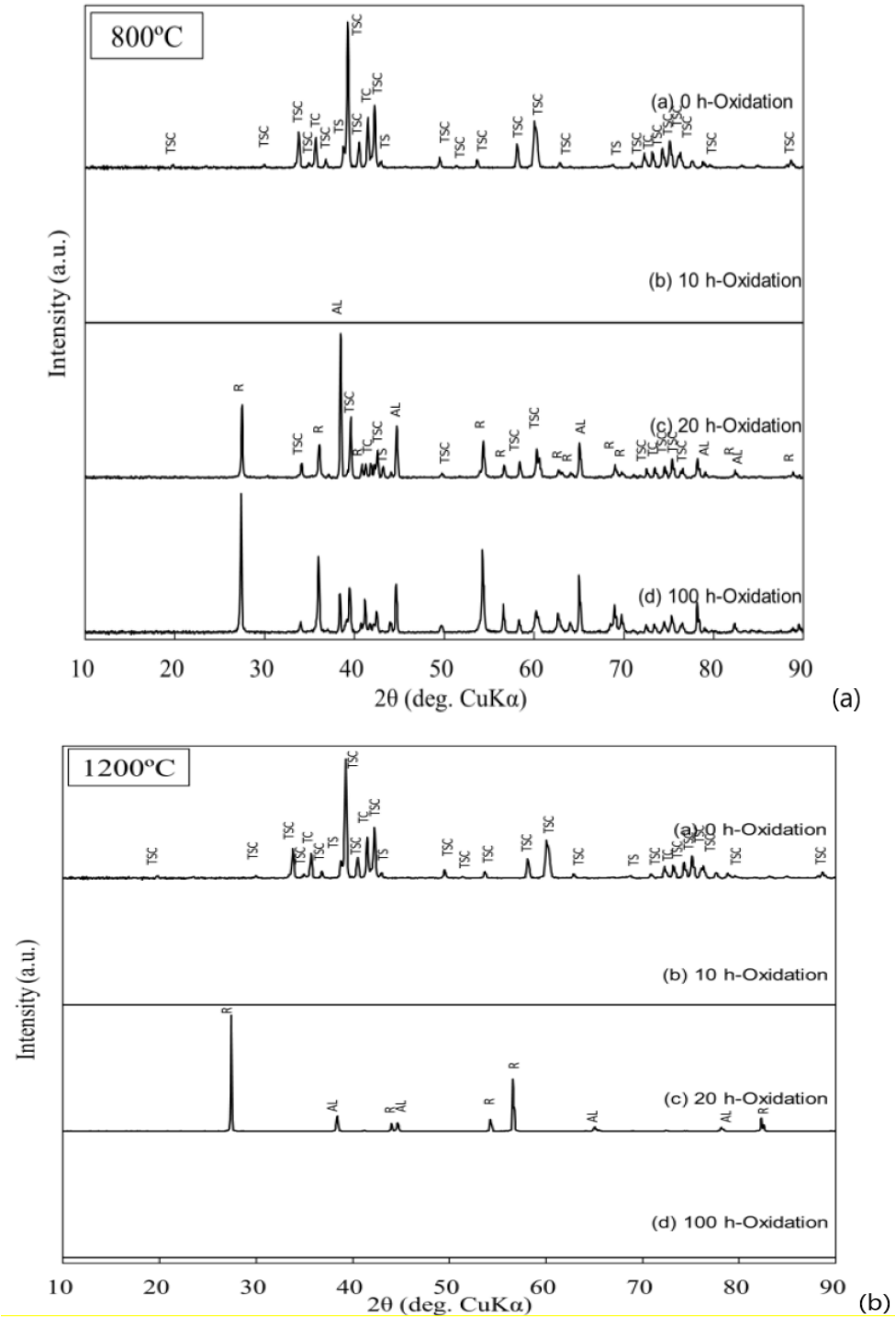

Figure 11. XRD patterns of TSC samples after water vapour corrosion at 800°C for 0, 20 and 100 h (b) XRD patterns for TSC samples after oxidation test at 1200°C for 0 and 20 h where Al: Aluminium, R: Rutile structured TiO_2, TS: $TiSi_2$, TC: TiC.

The chemical analysis using EPMA on the TSC samples prior to oxidation are shown in Figure 12. As seen in the Figure 12, the EPMA shows presence of Si, C and Ti. From the EPMA the TiC are spread out homogeneously throughout the TSC specimen. EPMA was conducted on three random points as shown in Fig. 12(b) and the compositions determined at the points are tabulated in Table 2. The phases belong to TiC, $TiSi_2$ and TSC which makes them the dominant material on the samples. The EPMA of the oxidised TSC samples at 800°C for the time of 20 h in the presence of water vapour shows the formation of thin (~125 μm) oxide layer. The EPMA shows presence of oxide layers formed by the elements of Ti, O and Si and as observed in TAC, there have been bulk clusters visible in the TSC which proves that the TiO_2 layers have clustered in the TSC samples. The observation from Fig. 13 leads to a conclusion that there is a formation of TiO_2 and SiO_2 mixed layer at shorter time intervals. The microstructure and oxide layer thickness of TSC specimen after oxidation at 1200°C for 20 h is seen in the Figure 14 (a & b). The elongated structure of the TSC is visible though SEM and an oxide layer of ~280μm is formed. The oxide layer thickness was uniform throughout the sample which proves that the material oxidises completely at temperature of 1200°C.

Table 2. Phase composition of TSC through EDAX

Point	C [at %]	Si [at %]	Ti [at %]	Phases
1	34.63	31.17	34.2	TS+TSC
2	41.42	1.01	57.56	TC
3	30.43	16.23	53.34	TSC

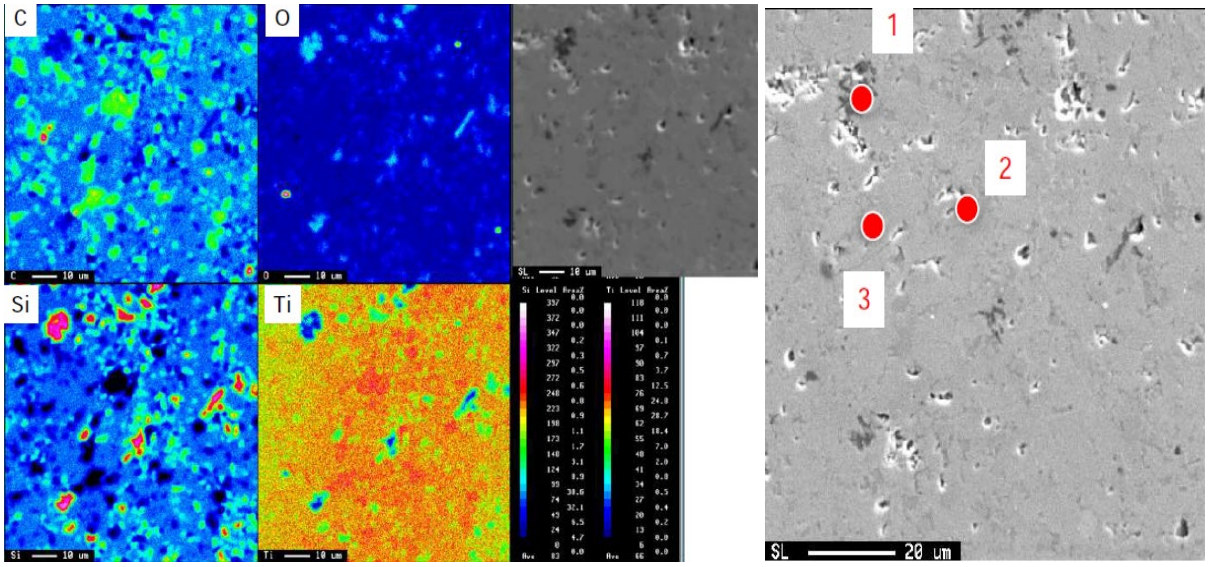

Figure 12. (a) EPMA of TSC specimen prior to oxidation (b) Three-point Analysis on TSC samples on EPMA

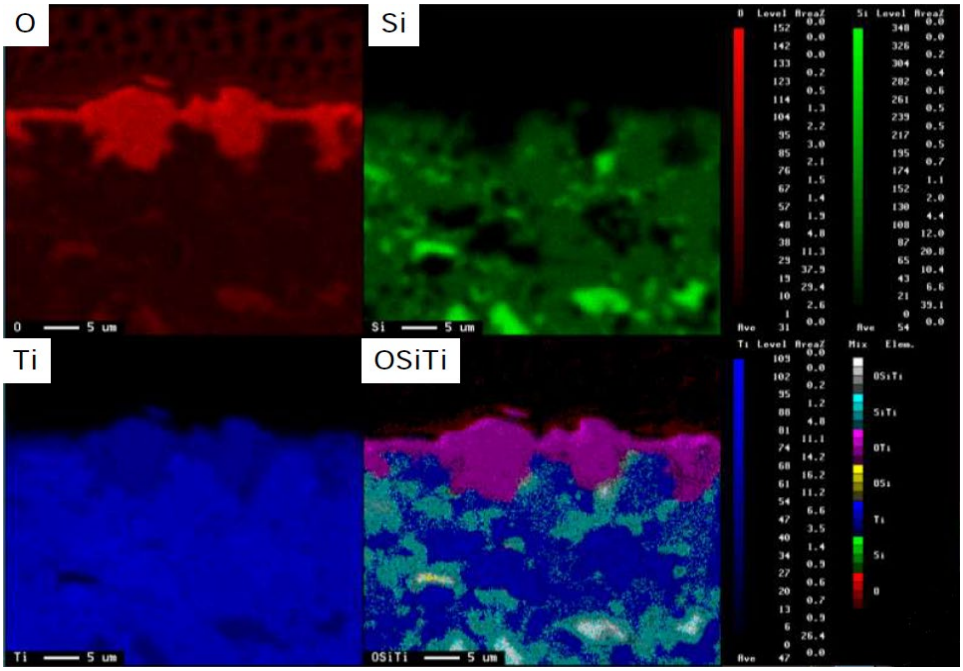

Figure 13. EPMA of the oxidised TSC sample at 1200°C/20 h

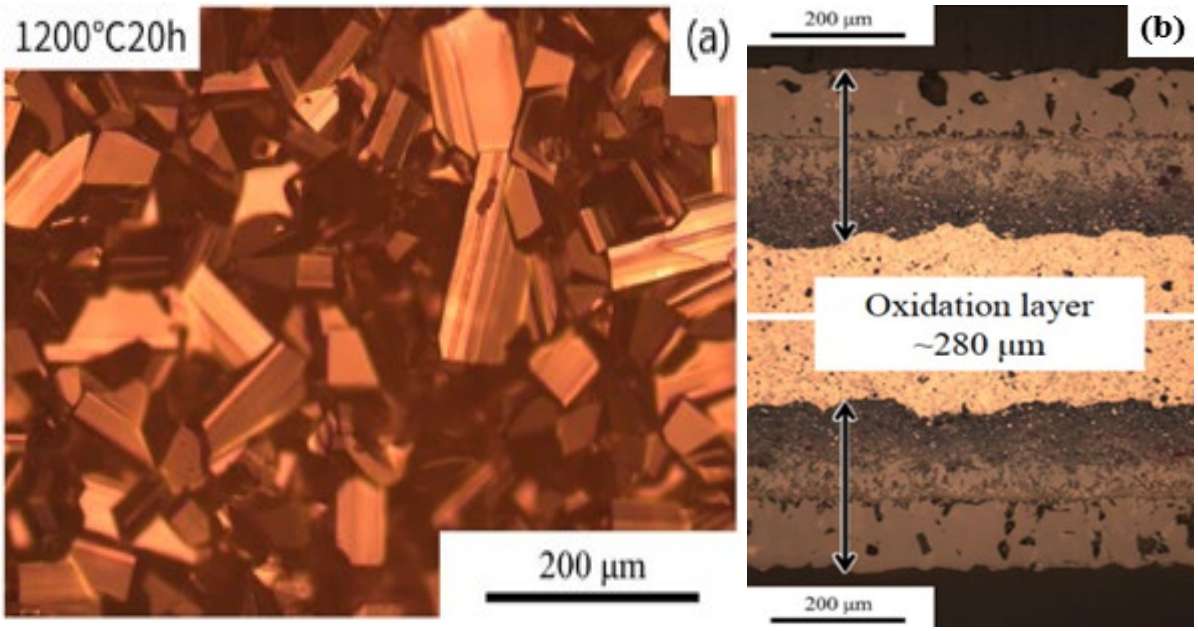

Figure 14. (a) Microstructure of TSC samples at 1200°C for 20 h (b) Oxidation layer on TSC samples due to water vapour corrosion at 1200°C for 20 h

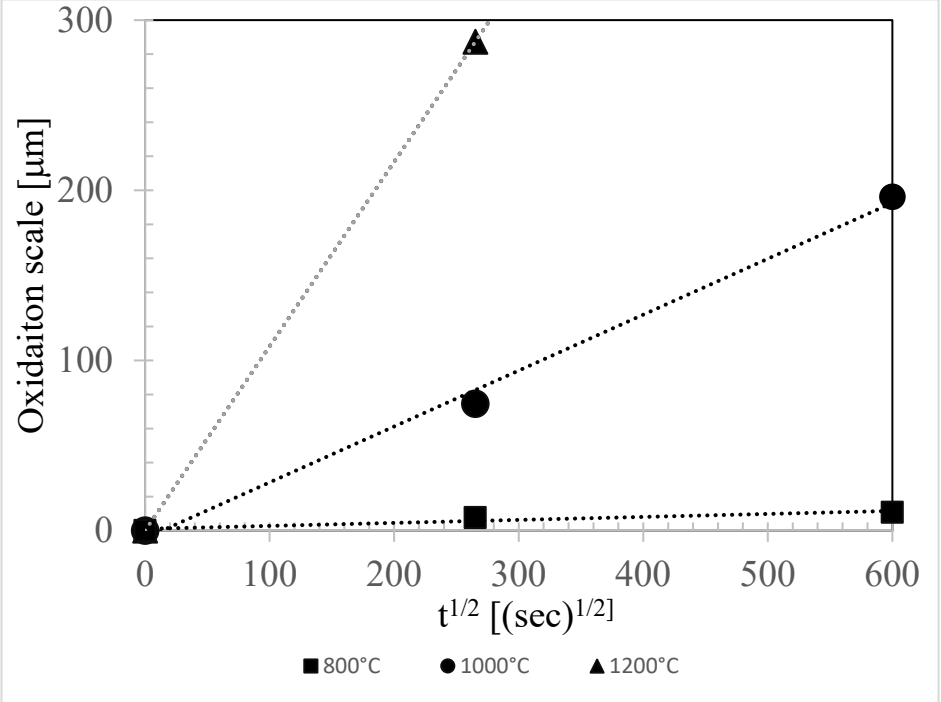

Figure 15. Oxidation growth of TSC samples

Figure 15 shows the oxidation kinetics of TSC samples. The material also follows the parabolic rate law of oxidation at the temperature of 800-1000°C in water vapour environment like the dry environment in steady state area [4]. The weight gain data was recorded as shown in Fig. 14 for different temperature and time. From Fig. 15, it was observed that the at higher

temperature the samples oxidised rapidly at shorter time intervals. At temperature intervals of 800 and 1000℃, the samples follow parabolic rate of oxidation law. But at 1200℃, certain samples were not retrieved from the furnace, but the samples retrieved at 20 hours shows a linear oxidation in water vapour environment which is different from dry environment. But comparing the oxidation kinetics and weight gain, the samples showed gain in mass exponentially due to formation of rutile phases of TiO_2 which leads to conclusion that the material oxidised vigorously in the water vapour environment owing to the formation of volatile $Si(OH)_4$.

Zhimei Sun *et al*. studied the oxidation behaviour of TSC samples under dry air condition and concluded that the specimen undergoes parabolic behaviour of oxidation until a temperature range of 1100℃, and after 1100℃ the material undergoes further oxidation forming a two-step oxidation process in temperature range of 1200-1300℃ which was not reported earlier [21]. D.B.Lee *et al*. reported the oxidation of TSC under air and stated that the material undergoes oxidation even in presence of air with higher weight change in the temperature of 1200℃ [22]. In this study, the oxidation behaviour of TSC was said to obey the parabolic law of oxidation until 1000℃ with higher diffusion rate followed with linear oxidation at 1200°C. It was said to be due to the outward diffusion of Ti present whereas O_2 underwent inward diffusion. The reaction of TSC specimen under water vapour environment at high temperatures was stated as below [23].

$$Ti_3SiC_2 + 10H_2O(g) \rightarrow 3TiO_2(s) + SiO_2(s) + CO(g) + 3H_2(g) \quad (7)$$

The equation provides a presence of SiO_2 which was not observed during the XRD or optical microscopy. It is believed that the SiO_2 formed reacted again with the water leading to the formation of $Si(OH)_4$ a volatile and corrosive material which could be responsible for high oxidation kinetics of TSC. The formation reaction of $Si(OH)_4$ through SiO_2 is given in equation (8).

$$SiO_2(s) + H_2O(g) \rightarrow Si(OH)_4(g) \quad (8)$$

The volatile $Si(OH)_4$ released from the surface of the TSC specimen would lead to formation of TiO_2 intermediate layers on the top surface of the TSC specimen. Even though, the intermediate layer of TiO_2 could provide a protective corrosion layer, in TAC samples, the protective layer formed though a mixture of TiO_2 and Al_2O_3 would give better protection in hot corrosion environment.

Evaluating the results obtained from the analysis, it can be inferred that both TAC and TSC follow parabolic law of oxidation at water vapour environment for certain period. The oxidation resistance of TAC was significantly better than the TSC in water vapour environment due to the protective layer formed with the mixture of TiO_2 and Al_2O_3. Although, TSC have good resistance towards oxidation in air by the formation of passive silica layer on the top, in water vapour environment, the formation of volatile $Si(OH)_4$ led to recession on the material leading to its poor resistance. Phase analysis, chemical and microstructural study also supported the better oxidation resistance of TAC under water vapour environment.

Mechanical Properties

Table 3. Results of Tensile & Fracture Strength

Material	Temperature	Tensile Strength (MPa)		Fracture Strength (MPa)
		Experimental	Calculated (FEA)	
TAC	RT	87.6	93.1	47.6
	288^0C	28.6	22.4	15.1
TSC	RT	76	83.8	77.1
	288^0C	190	183.6	207.8

Tensile properties of TSC and TAC samples at room and hydrothermal conditions are tabulated at Table 3. The tensile strength and fracture strength of TAC sample at room temperature was 87.6 MPa and 47.6 MPa, respectively whereas at hydrothermal condition of 288℃ and 250 bar of pressure, the strength drops more than 60% to 28.6 MPa and 15.1 MPa, respectively. Contrastingly, for TSC samples, the tensile strength at hydrothermal condition increased 60% from 76 MPa to 190MPa and the fracture strength increased from 77.1 to 207.8 MPa.

The room temperature tensile properties of the TAC and TSC samples were nearly similar as they exhibited same property of brittle nature of ceramics. Being a ceramic formed between the Ti and Al metal, the room temperature tensile strength of TAC was more as it exhibited more of metallic bond behaviour than TSC. But at hydrothermal condition, the strength of TSC were far greater than that of TAC. This increase in strength may have been possibly due to the rule of mixtures and bonding between the atoms. In TSC samples, the energy needed to break the covalent bond between the Si and carbide were higher which led to higher tensile and fracture strength. It is believed that at hydrothermal condition, the tensile strength of the material reduced due to the coarsening of grains which lead to cavitation on grain boundary

which reduce the ductility nature of the material [24]. Also, it was believed that as being a better oxidation resistance material TAC does not oxide at temperature of 288℃, so the formation of oxide layer may be limited leading to reduced tensile strength. But in case of TSC samples, the tensile strength at room temperature is closer to that of TAC specimen but at hydrothermal conditions, the tensile strength have increased over 60% from 76MPa to 190MPa. The covalent bond between the TSC samples may be the reason for higher tensile strength of the specimen. Also, the formation of oxide layer even at low temperature could also had effect on the tensile strength of the specimen. The Finite Element Analysis using the ANSYS 19.2 static structural conducted on the samples at both conditions lead to the conclusion that there is a variation of ±7% which may be due to the errors on the computer or working condition and machine heats which are possible dependents.

The finite element analysis using Ansys also supported the results obtained though the experimental method. Even though the results of FEA shown up some variation with the experimental results, the possibility of getting accurate result are closer to 1% as most of the FEA depends on the computer performance, mesh quality and user input. However, the results of experimental basically depends on the human factors and errors, environmental condition such as temperature, machine calibrations. So, the variance of 7% can be neglected. From FEA results, it can be concluded that the analytical method can possibly replace experimental work on studying complex structures and more difficult procedures which have human factors. Comparing both the samples tensile strength, the TSC strength at hydrothermal condition was far greater than TAC.

The bending strength of the samples was conducted before and after oxidation for 100 h. The stress-strain curves as shown in Fig 16 (a) of TAC reveal that the bending strength was not degraded due to the excellent oxidation resistance of TAC. No delamination was observed which would be otherwise due to the layered structured. In case of the TSC, the bending strength was maintained up to 800℃/100 h due to the presence of TSC in the specimen whereas at 1000℃, the XRD shows reduced phases of TSC which leads to reduced bending strength. The 1200℃ sample were not able to retrieve from the furnace which made to lack of results.

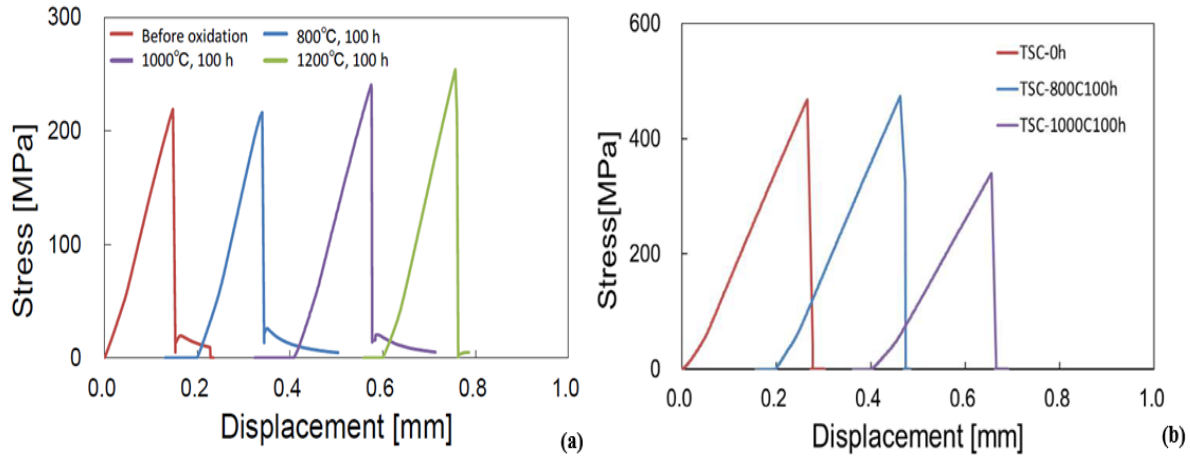

Figure 16. (a) Stress-Displacement curve for TAC specimen after bending strength and (b) Stress-Displacement curve for TSC samples

Although in case of TSC there have been a slight decrease at 1000°C sample. The retention of strength of TSC samples might be attributed to the formation of oxide layers of TiO_2 on top of the specimen leading to enhanced strength. The bend strength of both samples has not degraded leading to a discussion that both materials had formation of oxide layers on them. Figure 17 shows the Gibbs free energy of oxide formation in the samples of TAC and TSC. It can be said that the formation of α-Al_2O_3 and TiO_2 have the lowest Gibbs activation energy among all of the possible oxides which could be formed as observed by many researchers [25, 17]. In case of TAC samples, formation of Al is faster than Ti atoms, due to the metallic bond shared between the Ti_2C layer and Al layer. But in view of thermodynamics, the formation of α- Al_2O_3 and TiO_2 has negative Gibbs energy values. But since Al_2O_3 has more negative value of -432 KJ/mol, it forms faster than TiO_2 [26]. This may also be the reason for formation of Al in the TSC samples by reduction reaction. In TSC samples, the Ti and Si shares a covalent bond which is harder to break compared with metallic bond of Al.

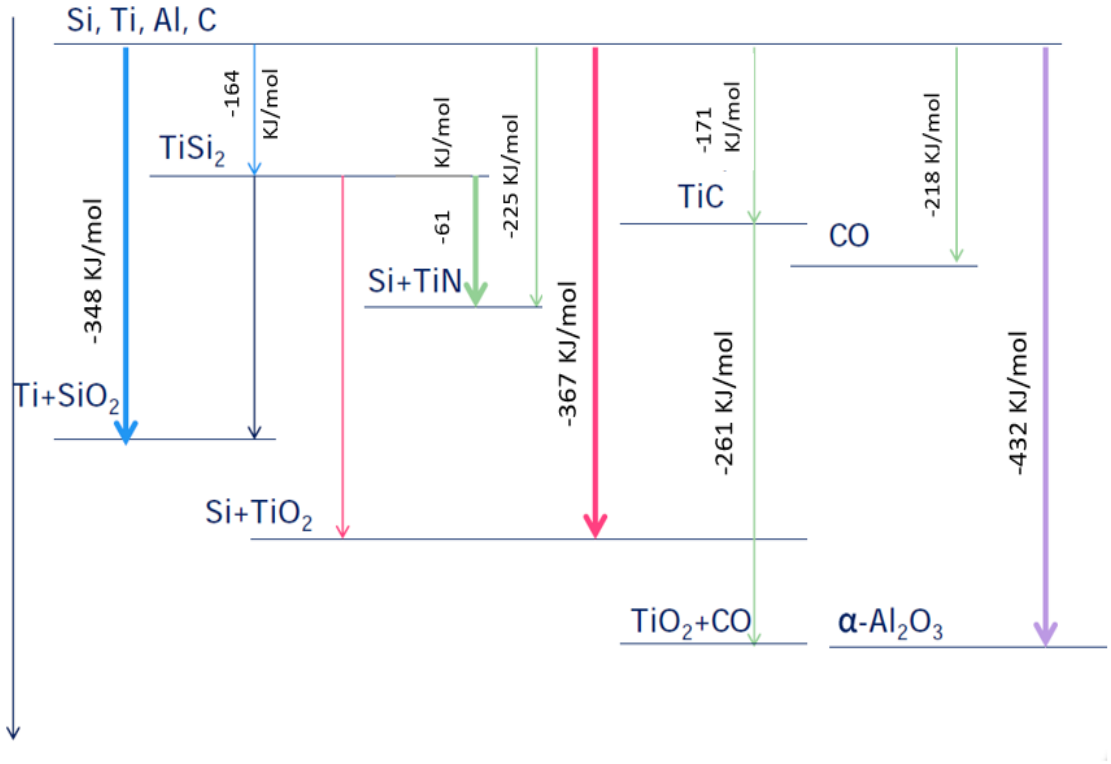

Figure 17. Gibbs Free energy of oxide formation for TAC and TSC samples

Oxidation Modelling

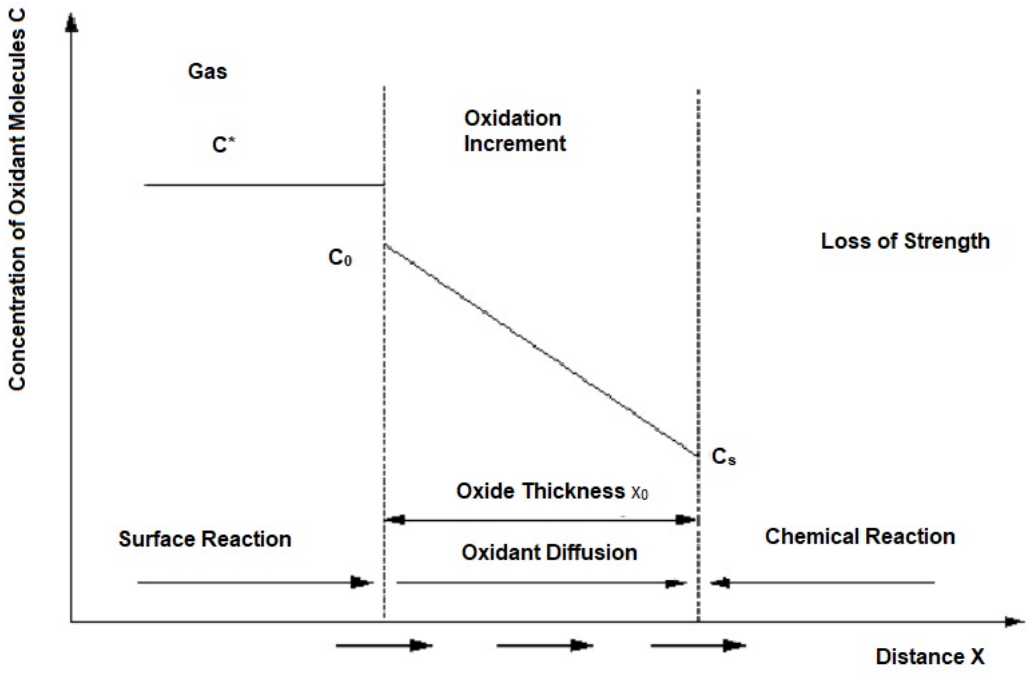

Figure 18. Oxidation region for metals and MAX phase materials

Oxidation of MAX phase ceramics is based on the physical phenomenon of molecular diffusions where the diffusion of oxygen, high temperature deformation, transient heat conduction and permanent swelling due to formation of product after reaction are common behaviour noted as shown in Fig 18 in high temperature alloys and metals [27]. In case of MAX phase ceramics, the first assumption to be considered would be the law of Lavoisier which states that mass can neither be created or destroyed which leads to assuming that there is no flow divergence.

$$\frac{\partial \rho}{\partial t} + \nabla \cdot J = 0 \tag{9}$$

Where ρ is the flow density which is a function of position vector ($\vec{r}$) and time (t) and J is the flux of substance that comes from one point to another. Also, the total flux in a continuum regime is defined as the rate of change of concentration or its gradients, Hence J is defined as,

$$J = -D\nabla\rho \tag{10}$$

Where D is diffusion constant that depends on the material. Taking the divergence of J leads to the equation (10) which is further combined with equation (9) leading to an equation with first order time and second order position derivative as shown in equation (12).

$$\nabla \cdot J = -D\nabla^2\rho \tag{11}$$

$$\frac{\partial \rho}{\partial t} + D\nabla^2\rho = 0 \tag{12}$$

By deriving the x and y components from equation (12)

$$\frac{\partial \boldsymbol{\rho}}{\partial \mathbf{t}} + \frac{\partial^2 \boldsymbol{\rho}}{\partial \boldsymbol{x}^2} = 0 \tag{13}$$

$$\frac{\partial \boldsymbol{\rho}}{\partial \mathbf{t}} + \frac{\partial^2 \boldsymbol{\rho}}{\partial \boldsymbol{y}^2} = 0 \tag{14}$$

The solution of equation (13) & (14) would have a time dependent part which will be a function of exponential and a position dependent part will be sinusoidal which is consistent with the fact of diffusion and conservation of mass that the part of material which diffuses into the other, it may not return to original state.

$$\boldsymbol{\rho}(\boldsymbol{r}, \boldsymbol{t}) = e^{At} \cdot [B \sin Dx + C \cos Dx\ ] \tag{15}$$

Where A, B and C are arbitrary constants and D is the diffusion constant. Diffusion of oxygen through solid material would be dry or wet condition. Both the condition cause loss/gain in the strength of within small particles and could appropriate to be linear in time and space. There is a similar loss/gain in weight during both the diffusion conditions even though the wet oxidation is faster than the dry oxidation. Considering the linear diffusion in the first order, the total flux is given by Flicks Law from equation (11) which corresponds to the rate of change in oxygen molecules

$$\boldsymbol{J_0 = D\frac{\partial C}{\partial r}} \tag{16}$$

With D being the diffusivity constant and C being the concentration of oxygen. Assuming diffusion happens only towards one direction (x- direction) the above partial differential equation is simplified in an ordinary differential equation, hence:

$$\boldsymbol{J = D\frac{dC}{dx}} \tag{17}$$

Now, the concentration of oxygen will be a function of X direction alone. The oxidation of the max phase was considered to take place in three different phases i.e. initial phase when the

material is being exposed into corrodent/oxidant, usually oxygen (O_2), a second phase , when initial diffusion of the oxygen within the material start and a layer with thickness (t_{ox}) is formed, and a third phase then the material start experience gain/loss of strength.Assuming C_g is the concentration of oxygen in the corrodent/oxidant and C_S the consternation at the boundary of the sample. The change in concentration dC of equation (11) can be written as:

$$\boldsymbol{dC = C_g - C_s} \tag{18}$$

Let the boundary layer thickness, leads to rate of change of concentration in the x-direction being given by:

$$\boldsymbol{\frac{dC}{dx} = \frac{C_g - C_s}{\delta}} \tag{19}$$

The parabolic nature of the diffusion and Flicks equation, a small layer the equation can be further simplified considering that the layer thickness can be written as a ratio of diffusion constant and heat mass transfer coefficient, Hence

$$D = \delta \cdot h_g \tag{20}$$

Equation (17) is therefore simplified as:

$$J_1 = \delta \cdot h_g \cdot \frac{C_g - C_s}{\delta} \tag{21}$$

$$J_1 = h_g \cdot (C_g - C_s) \tag{22}$$

The subscript 1 means that this flux is calculated as phase one gas. By Henry's Law, given a certain concentration, in the gas phase at the surface, amount of material will be absorbed under the surface. The Concentration at the surface C_0 is the partial pressure P_s, by the Ideal gas-law P_S is going to be the Concentration of gas at the surface C_s multiply the Boltzmann Constant (k) and the Temperature (T).

$$C_O = HP_S = HC_S kT \tag{23}$$

The second phase analogy to the first phase, the total flux will be given by linearized Diffusion Law. The flux of reacting through the oxide film will be given by:

$$J_2 = \frac{D}{t_{ox}}(C_s - C_i) \tag{24}$$

The oxygen will then react at the material point, and the flux of reactant will be given by:

$$J_3 = K_s C_i \tag{25}$$

With C_i be the concentration at the material interface and K_S the reaction rate constant. Assuming that material oxidation is the ultimate step and assuming that after a significant amount of time will reach a steady state, all the three fluxes can be equalized, hence:

$$J_1 = J_2 = J_3 = J_{SS} \tag{26}$$

Combining equation (17), (22) and (25) finds formulae for C_0 and C_i.

$$J_1 = J_3 \rightarrow h_g(C_g - C_s) = K_s C_i \tag{27}$$

Hence:

$$C_i = \frac{h_g}{K_s}(C_g - C_s) \tag{28}$$

Also:

$$J_1 = J_2 \rightarrow h_g(C_g - C_s) = \frac{D}{t_{ox}}(C_g - C_s) \tag{29}$$

$$h_g(C_g - C_s) = \frac{D}{t_{ox}}C_0 - \frac{D}{t_{ox}} \cdot \frac{h_g}{C_s}(C_g - C_s) \tag{30}$$

$$\frac{D}{t_{ox}}C_0 = h_g(C_g - C_s) + \frac{D}{t_{ox}} \cdot \frac{h_g}{C_s}(C_g - C_s) \tag{31}$$

Hence:

$$C_0 = \frac{t_{ox}}{D}h_g(C_g - C_s) + \frac{t_{ox}}{D}\frac{D}{t_{ox}} \cdot \frac{h_g}{C_s}(C_g - C_s) \tag{32}$$

$$C_0 = (C_g - C_s) \cdot [\frac{t_{ox}h_g}{D}h_g + \cdot \frac{h_g}{C_s}] \tag{33}$$

And

$$C_g = \frac{C_0}{\frac{t_{ox}h_g}{D}h_g + \frac{h_g}{C_s}} + C_s \tag{34}$$

Using Henry law to work out C_0 and using equation (24) leads to

$$J_2 = \frac{D}{t_{ox}}HC_s kT - \frac{D}{t_{ox}}\frac{h_g}{K_s}(C_g - C_s) \tag{35}$$

Combining equation (28) to (35)

$$J_2 = \frac{D}{t_{ox}} HC_s kT - \frac{D}{t_{ox}} \frac{h_g}{K_s} \left(\frac{C_0}{\frac{t_{ox} h_g}{D} h_g + \frac{h_g}{C_s}} \right) \quad (36)$$

Recalling J_{ss} is also J_2, the formula for steady state flux is given by

$$J_{SS} = \frac{HK_S P_g}{1 + \left(\frac{K_S}{h}\right) + \left(\frac{K_S t_{ox}}{D}\right)} \quad (37)$$

Where:

H= Henry's Constant

P_g = Partial Pressure of the reactant in the gas phase

h= mass transfer coefficient that depends on temperature

K_S= reaction rate constant

D= Diffusion Constant.

The purpose of the model is to find an equation that describe the change of oxide thickness (t_{ox}) as a function of time, hence the flux equation (37) needs to be converted as a growth rate equation. Recalling that the flux per unit area per unit time can be converted to thickness knowing the density of the oxygen N_1.

$$\frac{J_{SS}}{N_1} = \frac{dt_{ox}}{dt} \quad (38)$$

Therefore:

$$\frac{dt_{ox}}{dt} = \frac{HK_S P_g}{N_1 \left[1 + \left(\frac{K_S}{h}\right) + \left(\frac{K_S t_{ox}}{D}\right)\right]} \quad (39)$$

Equation (39) is a first order linear differential equation that can be solved by separation of variables.

$$N_1 \left[1 + \left(\frac{K_S}{h}\right) + \left(\frac{K_S t_{ox}}{D}\right)\right] dt_{ox} = HK_S P_g \, dt \quad (40)$$

Assuming the original thickness of layer is a certain quantity t_o and that the sample from time 0 to time t the oxidation thickness increased from t_0 to t_{ox} the equation can be integrated as follow:

$$\int_{t_0}^{t_{ox}} \left[1 + \left(\frac{K_S}{h}\right) + \left(\frac{K_S t_{ox}}{D}\right)\right] N_1 dt_{ox} = \int_0^t HK_S P_g \, dt \quad (41)$$

Solving this integral leads to:

$$\frac{K_s}{2D}(t_{ox}^2 - t_0^2) + \left(1 + \frac{K_s}{h}\right)(t_{ox} - t_o) = \frac{HK_sP_g}{N_1}t \quad (42)$$

Let:

$$A = 2D\left(\frac{1}{h} + \frac{1}{K_S}\right) \quad (42)$$

and

$$B = \frac{2DHP_g}{N_1} \quad (43)$$

And defining a new variable **τ** that is a function of initial oxide thickness.

$$\tau = \frac{t_0^2 - At_o}{B} \quad (44)$$

Equation (42) is simplified in a quadratic equation that, once solved, gives the total oxide thickness of the material subject to oxidation, this method is also known as Deal- Gove model and has been widely used in linear and parabolic oxidation of semi-conductor. Solution to this equation gives oxide thickness as a function of time.

$$t_{ox}^2 - At_{ox} = B(t + \tau) \quad (45)$$

Solving quadratic equation for t_{ox} is relatively simple as it is in the form $ax^2+bx+c=0$ hence, t_{ox} is given by:

$$t_{ox} = \frac{A \pm \sqrt{A^2 - 4B(t+\tau)}}{2} \quad (46)$$

A and B depends upon a series of constant that may not always be readily deductibles, however for wet and dry oxidation with water vapour or simply water, A and B can be worked out using the Arrhenius equation. The oxidation rate increases with higher temperature, and so the values of A and B must also increase. It was found experimentally that both A and B follow the Arrhenius law:

$$\mathrm{B} = \mathrm{C}_1 \cdot \mathrm{e}^{-\frac{E}{\mathrm{kT}}} \quad (47)$$

$$A = \frac{\mathrm{B}}{\mathrm{C}_2 \cdot \mathrm{e}^{-\frac{\mathrm{E}}{\mathrm{kT}}}} \quad (48)$$

Where C_1 and C_2 are the pre-exponential constant, k is the Boltzmann Constant and T is the temperature and E is the activation energy, for simple oxidation in water or oxygen these values are given in Table 4.

Table 4. C1 and C2 values for linear and parabolic oxidation

	Linear Oxidation	*Parabolic Oxidation*
Dry O_2	$C_1 = 7.72 \times 10^2$ μm²/hr	$C_2 = 6.23 \times 10^6$ μm²/hr
	E=1.23 eV	E= 2.00 eV
Wet H_2O	$C_1 = 3.86 \times 10^2$ μm²/hr	$C_2 = 6.23 \times 10^6$ μm²/hr
	E=0.78 eV	E= 2.05 eV

Linear Oxidation is when $\boldsymbol{\tau >> t}$ and there is a straight line of oxidation increasing. Parabolic oxidation is when $\boldsymbol{t \ll \frac{A^2}{4B}}$ and as a result therefore there is a sharp raise of oxidation.

Table 5. Results of parabolic and Linear oxidation thickness

Temperature (°C)	Time (hours)	Ti_2AlC		Ti_3SiC_2	
		Linear Oxidation (μm)	Parabolic Oxidation (μm)	Linear Oxidation (μm)	Parabolic Oxidation (μm)
800°C	10	0.229	0.092	0.284	1.29
	20	188.179	0.12	0.568	1.83
	100	940.88	0.28	2.84	4.09
1000°C	10	7.44	0.177	8.93	1.65
	20	14.88	0.251	17.86	2.34
	100	74.44	0.561	89.32	5.23
1200°C	10	94.08	0.287	110.14	1.98
	20	188.177	0.406	220.287	2.80
	100	940.88	0.910	1101.43	6.269

The Table 5 shows the oxidation thickness values calculated from the above derived Deal-Grove based mathematical model to valid the results obtained from the experimental method of water vapour corrosion. As described above, Ti_2AlC follows parabolic rate of oxidation with lower lesser diffusion whereas Ti_3SiC_2 ceramics followed the parabolic law until 1000°C after that the material is said to follow linear oxidation. The linear oxidation on the Ti_3SiC_2 was

verified by the result obtained through mathematically modelling along with oxidisation growth observed via SEM in Fig 14(b). The observed oxidation thickness was closer in range of 200µm. Even though the mathematical model assumed of infinite growth as well as no initial oxidation thickness in the sample. The results obtained from the model were closer to the oxidation thickness on the samples which shows that with further assumptions and research the model could be carried for future research.

Conclusion

The water vapour corrosion study on two MAX phase ceramics Ti_2AlC and Ti_3SiC_2 was conducted for different lengths of time at different temperatures from 800 to 1200°C. Both materials followed parabolic law of oxidation with Ti_2AlC having the excellent oxidation resistance with inward diffusion of oxygen whereas Ti_3SiC_2 showed signs of outward diffusion of oxygen leading to formation of TiO_2 phases on the top of surface. The retained bend strength after oxidation for 100h at 1000°C of Ti_2AlC did not degrade due to excellent oxidation resistance whereas in case of Ti_3SiC_2, there was a slight reduction in bend strength in 1000°C/100 h sample. The tensile strength of both samples at room temperature was nearly equal to one another but at hydrothermal condition due to presence of rutile TiO_2, the material TSC shown increased tensile strength which was also proven though finite element analysis. Mathematical modelling of the oxidation behaviour of the ceramics in dry and wet condition by Deal-Grove model suggested the parabolic and linear behaviour of oxidation in these ceramics. With certain assumptions the numerical results of the developed mathematical model are in line with the experimental findings showing that the Ti_3SiC_2 sample had higher oxidation thickness in the water vapour environment proving that the developed model is successful and could be further studied in future.

Declaration of competing interests

The authors declare that they have no known competing financial interests or personal relationship that could have appeared to influence the work reported in this paper.

Acknowledgement

One of the authors Karthikeyan would like to acknowledge the support provided by Kingston University, London towards his PhD studentship.

References

[1] Z.M.Sun, "Progress in research and development on MAX phases: a family of layered ternary compounds," *International Materials Reviews,* vol. 56, no. 3, pp. 143-166, 2011.

[2] J.L.Smialek, "Oxidation of Al_2O_3 Scale-Forming MAX Phases in Turbine Environments," *Metall and Mat Trans A,* vol. 49, pp. 782-792, 2018.

[3] S.P.Munagala, "MAX Phases: New Class of carbides and nitrides for aerospace structural applications," in *In: Prasad N., Wanhill R. (eds) Aerospace Materials and Material Technologies*, Singapore, Springer, 2017.

[4] N.C.Ghosh and S.P.Harimkar, "Microstructure and wear behavior of spark plasma sintered Ti_3SiC_2 and Ti_3SiC_2–TiC composites," *Ceramic International,* vol. 39, no. 4, pp. 4597-4607, 2013.

[5] M.Li, X.Zhou, H.Yang, S.Du and Q.Huang, "The critical issues of SiC materials for future nuclear systems," *Scripta Materialia,* vol. 143, pp. 149-153, 2018.

[6] E.N.Hoffman, D.W.Vinson, R.L.Sindelar, D.J.Talman, G.Kohse and M.W.Barsoum, "MAX phase carbides and nitrides: Properties for future nuclear power plant in-core applications and neutron transmutation analysis," *Nuclear Engineering and Design,* vol. 244, pp. 17-24, 2012.

[7] L.Guo, Z.Yan, X.Wang and Q.He, "Ti_2AlC MAX phase for resistance against CMAS attack to thermal barrier coatings," *Ceramics International,* vol. 45, no. 6, pp. 7627-7634, 2019.

[8] J. L.Smialek, "Environmental resistance of a Ti_2AlC-type MAX phase in a high pressure burner rig," *Journal of the European Ceramic Society,* vol. 37, no. 1, pp. 23-34, 2017.

[9] M.Barsoum and T.El-Raghy, "The MAX phases: Unique new carbide and nitride materials," *American Scientist,* vol. 89, no. 4, pp. 334-343, 2001.

[10] B. R. Maier, B. L, Garcia-Diaz, B. Hauch, L. C. Olson, R. L, Sindelar and a. K. Sridharan, "Cold spray deposition of Ti_2AlC coatings for improved nuclear fuel cladding," *Jounral of Nuclear Materials,* vol. 466, pp. 712-717, 2015.

[11] Y.C.Zhou and X.H.Wang, "High-Temperature Oxidation Behavior of Ti_2AlC in Air," *Oxidation of Metals,* vol. 59, no. 3/4, pp. 303-320, 2003.

[12] B.Cui, D.D.jayaseelan and W.E.Lee, "Microstructural evolution during high-temperature oxidation of Ti_2AlC ceramics," *Acta Materialia,* vol. 59, no. 10, pp. 4116-4125, 2011.

[13] B.Cui, D.D.Jayaseelan and W.E.Lee, "TEM study of the early stages of Ti_2AlC oxidation at 900 °C," *Scripta Materialia,* vol. 67, no. 10, pp. 830-833, 2012.

[14] X.H.Wang and Y.C.Zhou, "Oxidation behavior of Ti_3AlC_2 at 1000–1400 °C in air," *Corrosion Sciences,* vol. 45, no. 5, pp. 891-907, 2003.

[15] X.H.Wang and Y.C.Zhou, "Intermediate temperature oxidaiton beahviour of Ti_2AlC in air," *Jounral of materials research,* vol. 17, no. 11, pp. 2974-2981, 2002.

[16] Z.J.Lin, M.S.Li, J.Y.Wang and Y.C.Zhou, "Influence of water vapor on the oxidation beahviour of Ti_3AlC_2 and Ti_2AlC," *Scripta Materialia,* vol. 58, pp. 29-32, 2008.

[17] G.M.Song, V.Schnabel, C.Kwarkernaak, S. d. Zwaag and J.M.Schneider, "High temperature oxidation behaviour of Ti_2AlC ceramic at 1200°C," *Materials at high temperatures,* vol. 29, no. 3, pp. 205-209, 2012.

[18] T.Chen, P.M.Green, J.L.Jordon, J.M.Hampikian and N.N.Thadhani, "Oxidation of Ti_3SiC_2 Composites in Air," *Metallurgical and Materials Transactions A,* vol. 33, pp. 1737-1742, 2002.

[19] C.Racault, F.Langlais and R.Naslain, "Solid-state synthesis and characterization of the ternary phase Ti_3SiC_2," *Jounral of Materials Science,* vol. 29, pp. 3384-3392, 1994.

[20] O.Braaten, A.Kjekshus and H.Kvande, "The Possible Reduction of Alumina to aluminium using hydrogen," *JOM,* vol. 52, pp. 47-53, 2000.

[21] Z.Sun, Y.Zhou and M.Li, "Oxidation behaviour of Ti_3SiC_2-based ceramic at 900–1300°C in air," *Corrosion Science,* vol. 43, no. 6, pp. 1095-1109, 2001.

[22] S.W.Park and D.B.Lee, "Oxidation of Ti_3SiC_2 between 900 and 1200 °C in Air," *Oxiation of metals,* vol. 67, pp. 51-66, 2007.

[23] G.Liu, M.Li and Y.Zhou, “Effect of Na_2SO_4 and Water Vapor on the Corrosion of Ti_3SiC_2,” *Oxidation of Metals,* vol. 66, no. 1/2, 2006.

[24] I.Baker and D.J.Gaydosh, “Displacement Fringes in FeAl,” *Physica status solidi(a),* vol. 96, no. 1, pp. 185-190, 1986.

[25] D.Lengzdina, I.M.Robertson and H.K.Birnbaum, “Oxidation behavior of a single phase γ-TiAl alloy in low-pressure oxygen and hydrogen,” *Acta Materialia,* vol. 53, no. 3, pp. 601-608, 2005.

[26] D.R.Lide, Handbook of chemistry and Physics, New York: CRC Press, 2000.

[27] K. Loeffel, L. Anand and Z. M. Gasem, “On modeling the oxidation of high-temperature alloys,” *Acta Materialia,* vol. 61, no. 2, pp. 399-424, 2013.